Journal of The Electrochemical Society, **157** (2) H227-H230 (2010)
0013-4651/2009/157(2)/H227/4/$28.00 © The Electrochemical Society

Photoconductive Enhancement of Single-Layer Tin Oxide–Coated ZnO Nanowires

Chin-Ching Lin,[a] Yu-Wei Chen,[c] Mei-Ching Chiang,[a] Chia-Hua Lee,[b] Yung-Liang Tung,[b] and San-Yuan Chen[c,*,z]

[a]*Material and Chemical Research Laboratories and* [b]*Photovoltaics Technology Center, Industrial Technology Research Institute, 310 Chutung, Taiwan*
[c]*Department of Materials Science and Engineering, National Chiao Tung University, 300 Hsinchu, Taiwan*

In this study, zinc oxide nanowires (ZnO NWs) coated with crystalline tin oxide (SnO_2) by an ultrasonic spray pyrolysis were investigated. High resolution transmission electron microscopy analysis confirms that a continuous single SnO_2 layer of about 10 nm has been coated on the ZnO NWs. Photoconductivity measurements revealed that the ZnO NWs coated with the single uniform SnO_2 layer had a higher photoconductivity ratio by about a factor of 8 compared to the pristine ZnO NWs, attributed to the multi-photoexcited electrons. Under a steady radiation of UV light ($\lambda = 325$ nm), a substantial increase in the steady-state photocurrent is noticeable, suggesting that extra photoinduced charges are transferred from SnO_2 to ZnO NWs.
 [DOI: 10.1149/1.3271100]

Manuscript submitted August 5, 2009; revised manuscript received November 3, 2009. Published December 17, 2009.

Because of its numerous applications, for example, as a UV protection film, a transparent conducting oxide film, an electron-transport medium for solar cells, a biochemical sensor, and a photocatalyst, zinc oxide (ZnO) is an important photoelectronic semiconductor with a direct wide bandgap of 3.37 eV and a relatively large exciton binding energy of 60 meV at room temperature.[1-5] Furthermore, the physical properties of ZnO nanowires (NWs) can be dramatically changed by surface modification with selected organic, inorganic, and biological species such as Al_2O_3, TiO_2, and ZnS.[5-7] Such specialization usually leads to a significant enhancement in electronic, mechanical, or photoelectronic properties.[6,8,9]

Recently, ZnO NWs augmented with ultrathin coatings represent a new electrode structure for collecting electrons in photovoltaic devices.[10,11] Gubbala et al. reported the high electron-transport behavior of SnO_2 nanoparticles wrapping around SnO_2 NWs in dye sensitized solar cells (DSSCs).[12] SnO_2 plays a key role in the applications of gas sensors,[13-15] DSSCs, and transparent conductive coatings for electrodes, and many deposition techniques have been developed for SnO_2-based films, including chemical vapor deposition, sol–gel, sputtering, and evaporation.[16-18]

Chemical deposition has received much attention because of its excellent uniformity and precise element composition control of large-scale films and the ability to coat diverse structures or shapes. Aboaf et al. reported that SnO_2 films can be prepared by a gas-phase reaction of $SnCl_4$ with H_2O or by a gas-phase reaction of $SnCl_4$ with O_2 via a spray pyrolysis method.[19,20] SnO_2 thin films can be regarded as a layer consisting of many high quality nanoparticles in a nanoscale.

It is technologically possible to deposit or grow SnO_2-based thin or thick films with nanosized crystalline SnO_2.[21,22] Therefore, in this work, we report the photoelectric behavior of single-crystalline ZnO NWs coated with a conductive and uniform single SnO_2 layer by ultrasonic spray pyrolysis. This work is motivated by potential applications of the combined ZnO NWs/SnO_2 system.

Experimental

The ZnO NWs reported here were grown using a low temperature method.[23] An equimolar (0.01 M) aqueous solution of $Zn(NO_3)_2 \cdot 6H_2O$ and hexamethylenetetramine was prepared. Subsequently, Si substrates with a thin ZnO seeding layer (20 nm) were placed inside the solution at 95°C for 24 h. After removal from the aqueous solutions, the substrates were rinsed with distilled water and dried at 60°C. To deposit SnO_2 on ZnO NWs, the initial solution was prepared from 0.5 mol of stannous chloride ($SnCl_2$) in 1.0 L of deionized water. The deposition temperature (working temperature) was 360°C, and the deposition times were 0.5–2 min for all the depositions. The carrier gas flow rate was maintained at 20 L/min in air. The crystalline phase and structure of the synthesized SnO_2-coated ZnO NWs were characterized by X-ray diffraction (XRD) with Cu Kα radiation, field-emission-scanning electron microscopy (FESEM), and high resolution transmission electron microscopy (HRTEM) using a JEOL 2100 equipped with an energy dispersive X-ray spectrometer (EDS). For transmission electron microscopy (TEM) analysis, the material was ultrasonically dispersed in 2-propanol and dropped onto a holey-carbon-coated copper grid. To characterize the photocurrent, a UV lamp ($\lambda = 325$ nm) was used as a light source. The photocurrent was measured by a two-probe current–voltage (I-V) system using a Keithley 237 source measurement unit.

Results and Discussion

Figure 1a shows an FESEM image of the as-synthesized ZnO NWs following a saturation–precipitation mechanism.[20] The sizes of the ZnO NWs were 20–30 nm diameters and a few micrometer lengths, depending on the growth conditions. Figure 1b and c shows the image of ZnO NWs coated with single-layer and multilayer SnO_2 shells by the spray pyrolysis deposition (SPD) process, respectively. The XRD patterns of the ZnO NWs and the ZnO NWs@SnO_2 nanocomposite are shown in Fig. 1d. The distinct peaks corresponding to ZnO and SnO_2 are observed, and the major diffraction peaks of the coating specimen are consistent with the known tetragonal SnO_2 structure with lattice constants given as $a = 4.755$ Å and $c = 3.199$ Å (JCPDS 41-1445). The main (200) peak intensity of the tetragonal SnO_2 increases with an increase in the coating layer, indicating that a better crystallinity of the shell layer can be obtained from the spray pyrolysis ZnO/SnO_2 NW. Given this condition, it can be concluded that the coated SnO_2 layers retain their perfect crystalline phase and physical structure, further confirming that a ZnO/SnO_2 NW nanocomposite, rather than an alloy, was formed.

The low magnification TEM image in Fig. 2a indicates that the NWs were completely covered with a single SnO_2 layer composed of SnO_2 nanoparticles. The diameter of the NWs was estimated to be about 25 nm, and the thickness of the coating layer was about 10 nm. From the XRD spectrum shown in Fig. 1d, the average size of SnO_2 nanoparticles calculated by the Scherrer equation was about 8 nm, consistent with the TEM results. The corresponding high magnification TEM image in Fig. 2b clearly shows that the SnO_2 nanoparticles were crystalline and distributed well on the NWs. The EDS spectrum in Fig. 2c obtained by focusing an electron beam with a

* Electrochemical Society Active Member.
z E-mail: sanyuanchen@mail.nctu.edu.tw

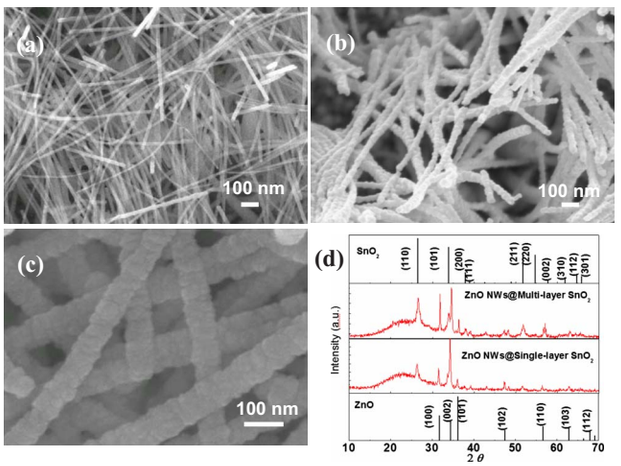

Figure 1. (Color online) Scanning electron microscopy micrographs of (a) ZnO NWs, (b) ZnO NWs coated with a thin SnO_2 layer (~10 nm), and (c) ZnO NWs coated with a thick SnO_2 layer (~40 nm). (d) XRD patterns of SnO_2-coated ZnO NWs.

spot size of 5.0 nm directly on the coated ZnO NWs clearly indicated tin, oxygen, and a significant zinc peak after a long acquisition time.

A typical structure for an *I-V* measurement consisting of Ag metal/ZnO NWs/SnO_2-coated ZnO NWs/ZnO NWs/Ag metal is presented schematically in Fig. 3a. Pristine ZnO NWs present a high resistivity of hundreds of megaohms that is about 2 orders of magnitude larger than that (above 3.5 MΩ) reported for naked single ZnO NWs. In contrast, as shown in Fig. 3b, as the SnO_2 layer was coated on the ZnO NWs, the device with the SnO_2 layer-modified ZnO NWs presented a different degree of conduction depending on the coating thickness of the SnO_2 layer. A single SnO_2 layer of ~10 nm on the surface of ZnO NWs could increase the current of the NW device by 30%, and with an increase in coating thickness, an enhanced conduction of as large as 150% could be obtained for the ZnO NWs coated with thick layers of SnO_2 (~40 nm). This improvement in the transport characteristics of the ZnO

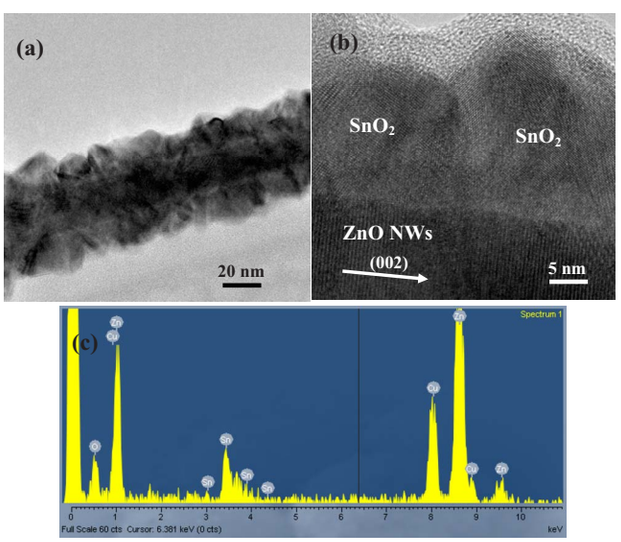

Figure 2. (Color online) (a) TEM image and (b) HRTEM micrograph of ZnO NWs coated with a single SnO_2 layer (~10 nm). (c) Element composition analysis of an individual ZnO NW@SnO_2.

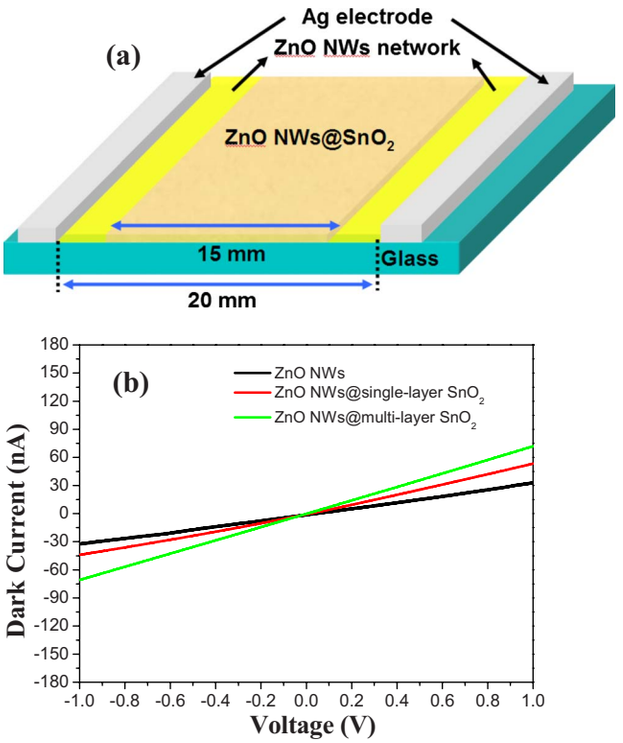

Figure 3. (Color online) (a) *I-V* measurement structure of ZnO NWs@SnO_2. (b) Room-temperature *I-V* curves of pristine ZnO NWs and ZnO NWs@SnO_2.

NWs@SnO_2 nanocomposite can be attributed to the decreased partial resistance of ZnO NWs and the increased probability of having many electrically conducting paths.

Figure 4 shows the photoresponse of ZnO NWs coated with various thicknesses of SnO_2 under modulated illumination of 325 nm wavelength light. Before the SnO_2 deposition, the dark current of ZnO NWs was very small ($I \sim 31$ nA@0.8 V) before illumination, but after the illumination was turned on, all the ZnO NW samples had a consistent current. This is the well-observed subbandgap photoconductivity in ZnO that corresponds to the generation of electron–hole pairs via optical transitions between defect states and the bandedge.[24] However, after SnO_2 deposition, the current (I) (the dark current) was enhanced for the ZnO NWs with the thin SnO_2 coating (i.e., 10 nm SnO_2-coated ZnO NWs, Fig. 4b). This behavior is attributed to the transfer of the photoexcited electrons from the conduction band of SnO_2 to that of ZnO, which is favorable for SnO_2 because the position of the lowest unoccupied energy level in SnO_2 is just above the lowest unoccupied energy level of ZnO. This is a strong evidence of a photosensitization effect because SnO_2 can provide additional electrons that are excited by short UV wavelengths ($\lambda < 360$ nm). However, ZnO NWs with a thicker SnO_2 (~40 nm) coating have a lower photoexcitation (1/3 time) than the pristine ZnO NWs, suggesting that the thicker SnO_2 absorbs most of the UV irradiation and acts as a shielding layer on ZnO NWs. To quantify the current enhancement, the transient photocurrent of the samples was analyzed. In the analysis, the starting time, $t = 0$, was set as the time when the UV irradiation and the current were measured up to $t = 30$ s so that the photoresponse current could be fully observed. It can be seen in Fig. 4 that after illumination the current rose rapidly before reaching a steady state and then decreased gradually. For the ZnO NWs and NWs@SnO_2 nanocomposite, the steady-state photocurrent started to decrease gradually after roughly 30 s of illumination. This phenomenon was mostly observed for the ZnO exposed in air (for pure ZnO) due to surface-related photoconduc-

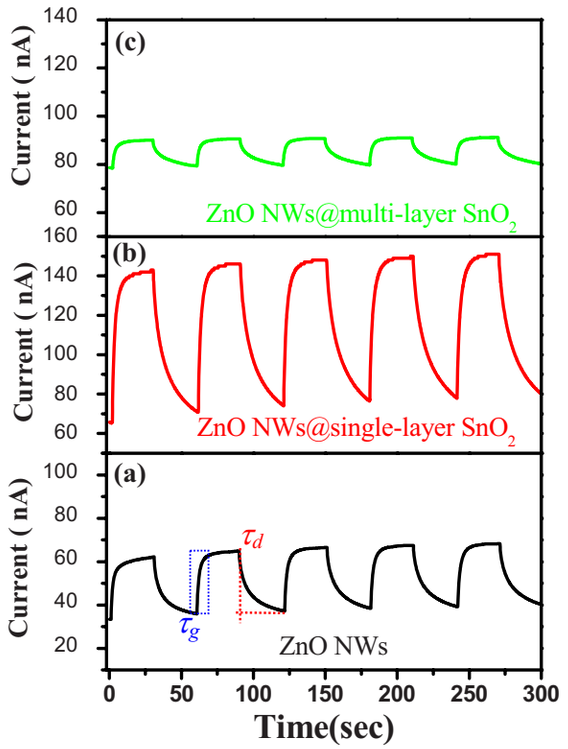

Figure 4. (Color online) Time dependence of the photocurrent with periodic irradiation of the light under continuous illumination of 325 nm in air at a bias voltage of 0.8 V for (a) ZnO NWs, (b) ZnO NWs@single-layer SnO_2, and (c) ZnO NWs@multilayer SnO_2.

tion, which is primarily governed by the desorption and adsorption of oxygen.[25] The response times of the photogeneration were estimated to be τ_g = 1.2, 2.0, 1.5 s in the initial growing stage for the ZnO NWs, the ZnO NWs@single-layer SnO_2, and the ZnO NWs@multilayer SnO_2, respectively. The increase in τ_g after SnO_2 deposition may be explained in terms of the effect of electron trapping on the achievement of a steady-state current after illumination. In the ZnO NW network, the number of electrons reaching the electrode determines the measured current under a constant bias voltage. However, the conducting electrons can be captured at trap centers. As a result, the starting time for photocurrent generation was slowed because the steady-state current could be reached only after all the traps were filled, a delay determined by the trap filling times of ZnO and the SnO_2 single layer. Under this condition, an equilibrium between multiple electron trapping and detrapping events was observed. In contrast, for the ZnO NWs@single-layer SnO_2 samples, the single SnO_2 layer provided additional electron traps to increase τ_g. After the illumination is turned on, the traps in SnO_2 must be filled before the photoelectrons can be injected into ZnO. As shown in Fig. 4, the time (τ_d) for photocurrent decay from the steady state to the dark current after UV irradiation was estimated to be about 25.6 s for ZnO NWs, but it could be decreased with a single-layer SnO_2 coating on the ZnO NWs. The reduction in τ_d implied that the thin SnO_2 layer played a significant role in surface photoconduction by providing partial passivation to minimize the interaction of oxygen with the ZnO surface.

A schematic energy band diagram is shown in Fig. 5 for the photoconduction mechanism in the presence of the ZnO NWs@SnO_2 nanocomposite. In this diagram, χ_{ZnO} is the electron affinity of n-type ZnO (~4.5 eV) and $E_{g\text{-}ZnO}$ is the bandgap of ZnO (~3.3 eV). Also, χ_{SnO_2} is the electron affinity of SnO_2 (~4.4 eV) and $E_{g\text{-}SnO_2}$ is the bandgap of SnO_2 (~3.6 eV).[26] Because of a slight band mismatch in this system, the barrier height

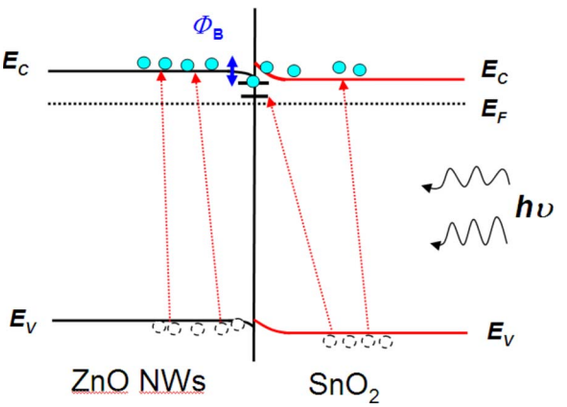

Figure 5. (Color online) Energy bands for SnO_2-coated ZnO NWs after UV irradiation.

becomes large and electrons are blocked in the ZnO region. The barrier height can be represented by $\Phi_B = (\chi_{ZnO} - \chi_{SnO_2})$ and calculated to be 0.1 eV. The trapping at the surface states drastically affects the transport of high surface-to-volume ratio nanostructured materials. Upon illumination by photons of energy larger than the semiconductor bandgap (E_g), electrons are excited into the conduction band in both parts of ZnO NWs and the single SnO_2 layer (~10 nm). Therefore, from this work it can be concluded that electron-transport properties can be controlled by depositing a SnO_2 layer on ZnO NWs that can then be used as three-dimensional electrodes to increase the conversion efficiency for photovoltaic devices.

Conclusion

We have developed a method to uniformly coat a single SnO_2 layer on ZnO NWs by an SPD process. A crystalline SnO_2-coated layer with a thickness of about 10 nm can be obtained, as confirmed by the HRTEM image of ZnO NWs@SnO_2. Transport measurements show that the photocurrent in ZnO NWs can be enhanced by multi-photoexcited electrons attributed to ZnO and the single SnO_2 layer under UV irradiation. The results presented in this study can pave the way toward the design of one-dimensional nanostructures for new possibilities in multifunctional nanodevices.

Acknowledgment

The authors gratefully acknowledge the financial support of the Industrial Technology Research Institute through grant no. 8301XS4710.

National Chiao Tung University assisted in meeting the publication costs of this article.

References

1. S. Choopun, R. D. Vispute, W. Noch, A. Balsamo, R. P. Sharma, T. Venkatesan, A. Iliadis, and D. C. Look, *Appl. Phys. Lett.*, **75**, 3947 (1999).
2. C. C. Lin, S. Y. Chen, S. Y. Cheng, and H. Y. Lee, *Appl. Phys. Lett.*, **84**, 5040 (2004).
3. M. H. Huang, S. Mao, H. Feick, H. Q. Yan, Y. Wu, H. Kind, E. Weber, R. Russo, and P. D. Yang, *Science*, **292**, 1897 (2001).
4. M. H. Huang, Y. Y. Wu, H. Feick, N. Tran, E. Weber, and P. D. Yang, *Adv. Mater.*, **13**, 113 (2001).
5. T. Y. Liu, H. C. Liao, C. C. Lin, S. H. Hu, and S. Y. Chen, *Langmuir*, **22**, 5804 (2006).
6. C. S. Hsiao, W. L. Kuo, S. Y. Chen, J. L. Shen, C. C. Lin, and S. Y. Cheng, *J. Electrochem. Soc.*, **155**, K96 (2008).
7. J. H. Choi, D. Y. Khang, and J. M. Myoung, *Solid State Commun.*, **148**, 126 (2008).
8. K. S. Leschkies, R. Divakar, J. Basu, E. E. Pommer, J. E. Boercker, C. B. Carter, U. R. Kortshagen, D. J. Norris, and E. S. Aydil, *Nano Lett.*, **7**, 1793 (2007).
9. A. J. Mieszawska, R. Jalilian, G. U. Sumanasekera, and F. P. Zamborini, *Small*, **3**, 722 (2007).
10. M. Knez, K. Nielsch, and L. Niinistö, *Adv. Mater.*, **19**, 3425 (2007).
11. S. K. Tripathy, T. Sahoo, I. H. Lee, and Y. T. Yu, *Mater. Lett.*, **61**, 4690 (2007).
12. S. Gubbala, V. Chakrapani, V. Kumar, and M. K. Sunkara, *Adv. Funct. Mater.*, **18**,

2411 (2008).
13. X. Song, Z. Wang, Y. Liu, C. Wang, and L. Li, *Nanotechnology*, **20**, 075501 (2009).
14. L. C. Tien, D. P. Norton, B. P. Gila, S. J. Pearton, H. T. Wang, B. S. Kang, and F. Ren, *Appl. Surf. Sci.*, **253**, 4748 (2007).
15. S. W. Choi, J. Y. Park, and S. S. Kim, *Nanotechnology*, **20**, 465603 (2009).
16. T. N. Blanto and M. Lelental, *Mater. Res. Bull.*, **29**, 537 (1994).
17. K. Y. Rajpure, M. N. Kusumade, M. N. Neumann-Spallart, and C. H. Bhosale, *Mater. Chem. Phys.*, **64**, 184 (2000).
18. C. C. Lin, M. C. Chiang, and Y. W. Chen, *Thin Solid Films*, **518**, 1241 (2009).
19. A. Aboaf, V. Marcotte, and N. Chou, *J. Electrochem. Soc*, **120**, 701 (1973).
20. M. Nagano, *J. Cryst. Growth*, **67**, 639 (1984).
21. J. Sanz Maudes and T. Rodriquez, *Thin Solid Films*, **69**, 183 (1980).
22. N. Barsan, M. Schweizer-Berberich, and W. Göpel, *Fresenius' J. Anal. Chem.*, **365**, 287 (1999).
23. L. Vayssieres, *Adv. Mater.*, **15**, 464 (2003).
24. C. C. Lin, C. S. Hsiao, S. Y. Chen, and S. Y. Cheng, *J. Electrochem. Soc.*, **151**, G285 (2004).
25. K. Keem, H. Kim, G. T. Kim, J. S. Lee, B. Min, K. Cho, M. Y. Sung, and S. Kim, *Appl. Phys. Lett.*, **84**, 4376 (2004).
26. D. Fröhlich, R. Klenkies, and R. Helbig, *Phys. Rev. Lett.*, **41**, 1750 (1978).